

Strong Proton–Electron Coupling in π -Planar Metal Complex with Redox-Active Ligands

Pingping Huang,^[a] Yukihiro Yoshida,^{*[a]} Yoshiaki Nakano,^[a,b] Hideki Yamochi,^[a,b] Mikihiro Hayashi,^[c] Hiroshi Kitagawa^{*[a]}

[a] P. Huang, Prof. Y. Yoshida, Dr. Y. Nakano, Prof. H. Yamochi, Prof. H. Kitagawa
Division of Chemistry, Graduate School of Science
Kyoto University
Kitashirakawa-Oiwakecho, Sakyo-ku, Kyoto 606-8502, Japan
E-mail: yoshiday@ssc.kuchem.kyoto-u.ac.jp, kitagawa@kuchem.kyoto-u.ac.jp

[b] Dr. Y. Nakano, Prof. H. Yamochi
Research Center for Low Temperature and Materials Sciences
Kyoto University
Kitashirakawa-Oiwakecho, Sakyo-ku, Kyoto 606-8501, Japan

[c] Dr. M. Hayashi
Faculty of Education
Nagasaki University
1-14 Bunkyo-machi, Nagasaki 852-8521, Japan

Supporting information for this article is given via a link at the end of the document.

Abstract: Proton-coupled electron transfer (PCET) of metal complexes has been widely studied, especially in biochemistry and catalytic chemistry. Although metal complexes bearing redox-active ligands play a part in these research areas, those with π -planar structure remain entirely unexplored, which are vital for future development of iono-electronics. Here, proton–electron coupling of a π -planar nickel complex bearing redox-active N,S-ligands, Ni(itsq)₂, was investigated by combining experimental and theoretical approaches. Strong proton–electron coupling was manifested in a large potential shift, which is twice greater than that of a typical PCET-type π -planar metal complex with redox-inactive ligands, [Ni(dcpdt)₂]²⁻. Theoretical calculations affirmed that the stabilization of frontier orbitals by protonation is greater in Ni(itsq)₂ than that in [Ni(dcpdt)₂]²⁻. These results indicate that π -planar metal complexes with redox-active ligands are promising for developing novel PCET-type materials.

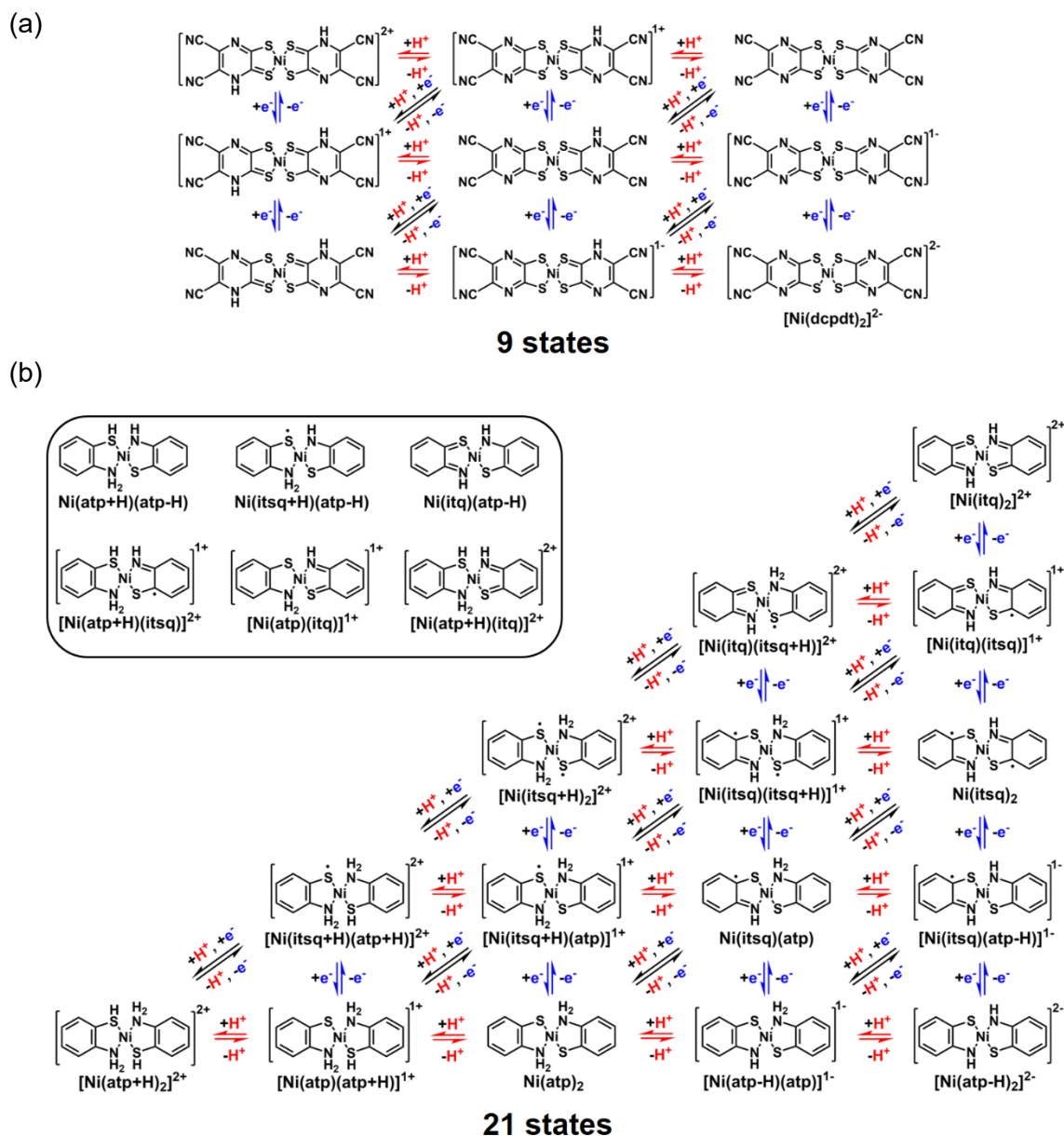
Proton-coupled electron transfer (PCET) plays a pivotal role in biology.^[1] For example, charge separation through PCET generates an electrochemical proton gradient for adenosine triphosphate (ATP) production in the energy conversion systems of biological cells. Proton pumping, coupled with electron transfer, is activated in photosystem II and cytochrome *c* oxidase.

In materials science, the PCET process has also attracted much attention as its potential contribution to unique electronic properties in the π -conjugated crystalline state,^[2] such as metallic behavior induced by hydrogen bonding interactions^[2c] and ferroelectric behavior associated with quantum proton fluctuations.^[2e] Metal complexes have excellent designability compared to organic compounds owing to the facile chemical modification of ligands and the diverse combinations of metals and ligands. Among them, metal complexes with π -planar structure have been the subject of extensive research for designing electronic materials including superconductors and quantum magnets.^[3] To date, many efforts have been devoted to elucidating the interactions between central metals and Lewis acidic/basic ligands in PCET-type π -planar metal complexes, in which the metal ion as a redox-active center can have various

valence states (Scheme 1a).^[4] Compared to redox-active metal ions, redox-active (so-called “non-innocent”) ligands are more promising for controlling the proton–electron coupling in metal complexes, because their chemical modification is expected to have a drastic effect not only on the Lewis acidity/basicity, but also on redox properties.^[5] However, the proton–electron coupling behavior of π -planar metal complexes having redox-active ligands has not yet been accomplished, although π -planarity being vital for the development of coherent proton-coupled electron transfer in iono-electronic systems.^[6]

o-Phenylenediamine as a typical redox-active ligand, which has three relatively stable redox states (i.e., diiminobenzoquinone, diiminosemiquinone, and diiminophenolate),^[5b,7] is known to undergo the multiproton/multielectron transfer process accompanied by π -reconstruction in response to protonation.^[8] For example, octahedral transition metal complexes bearing *o*-phenylenediamine ligands have been investigated as hydrogen production/storage materials using the multistep redox processes.^[8c,8d] However, the pH dependence of the redox potential is almost constant in π -planar metal complexes with diiminosemiquinone ligands,^[9] indicating the little proton–electron coupling.

In this study, we focused on a metal complex bearing a redox-active *o*-iminothiosemiquinonate (itsq¹⁻) ligand as a possible candidate for strong PCET systems (Scheme 1b and Figure S1). Compared with the aforementioned N,N-donor ligand, the N,S-donor ligand can promote the reconstruction of the π -conjugated system upon protonation (Figure 1a), because of the expanded orbital on sulfur atoms. In relation, the sulfur atom has a stronger σ and π donating ability than nitrogen, which stabilizes the complexation with a metal ion and improves the electron reservoir properties of the complex. It is noteworthy that the divalent metal complex can possess 21 kinds of possible redox/protonated states (Scheme 1b), which are much greater than those in metal complexes with redox-inactive ligands. For example, there are 9 kinds of possible redox/protonation states in a π -planar nickel complex with redox-inactive ligands, [Ni(dcpdt)₂]²⁻ (dcpdt²⁻: 5,6-dicyano-2,3-pyrazinedithiolate),^[4e,4f] as shown in Scheme 1a. Using experimental and theoretical methods, it was found that the



Scheme 1. Sequential proton transfer (red arrows), electron transfer (blue arrows), and proton-coupled electron transfer (black arrows) in (a) nickel complex with redox-inactive 5,6-dicyano-2,3-pyrazinedithiolate ligands (9 states)^[4] and (b) nickel complex with redox-active *o*-aminobenzenethiolate ligands (21 states), where complexes with positively charged ligands are excluded. In (b), states included in an upper left box (6 states) are regarded as those formed by intramolecular proton and/or electron transfer in a state drawn in the diagram (15 states).

π -planar nickel(II) complex, Ni(itsq)₂, showed a significant level of proton–electron coupling, which is comparable to that of [Ni(dcpdt)₂]²⁻. In this paper, the changes in the lowest unoccupied molecular orbital (LUMO) energy and reduction potential of Ni(itsq)₂ by protonation are mainly compared with those in the highest occupied molecular orbital (HOMO) energy and oxidation potential of [Ni(dcpdt)₂]²⁻, because they can be regarded as electron acceptor^[10] and electron donor,^[4e,4f] respectively.

Theoretical calculations using density functional theory (DFT) method with the RB3LYP functional revealed that the LUMO of Ni(itsq)₂ was mainly distributed on the ligands, in contrast to the HOMO (Figure 1b). Compared with electron-donating [Ni(dcpdt)₂]²⁻, proton and electron acceptances in electron-

accepting Ni(itsq)₂ result in a significant modification, not only of the LUMO energy level, but also in the distribution of the LUMO in the complex molecule. In particular, the contribution of the benzene rings to the LUMO is dramatically reduced, while that of the N,S-part increases. The calculation results stimulated us to investigate the PCET behavior associated with the reduction of Ni(itsq)₂ in order to clarify the effect of the redox-active ligands on proton–electron coupling in the metal complex. It was noted that the central Ni atom bears a positive charge ($q = +0.24$) and was occupied by 9.75 electrons ($3d^{8.83} 4s^{0.39} 4p^{0.53} 4d^{0.01}$), based on natural population analysis (NPA).^[10a] The excess charge over the formal 3d⁸ configuration arises from charge transfer from the ligands to the central nickel ion via the strong σ donation of sulfur

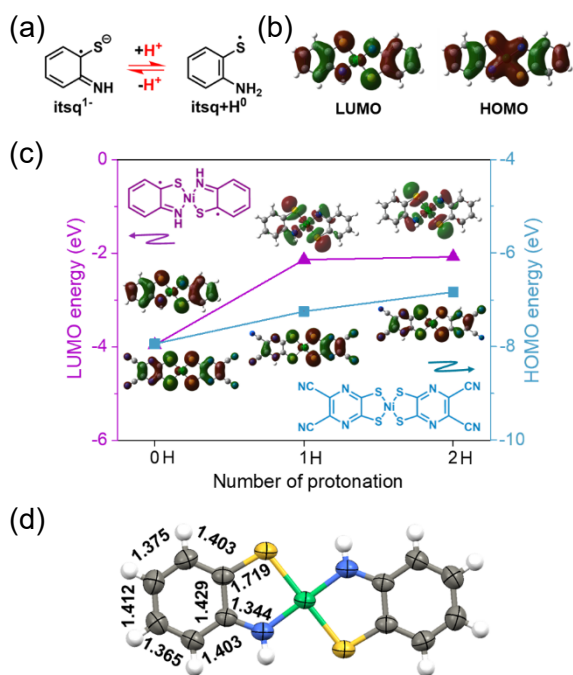


Figure 1. (a) π -Reconstruction of an itsq ligand in protonation/deprotonation processes. (b) Frontier orbitals, HOMO (right) and LUMO (left), of $\text{Ni}(\text{itsq})_2$ calculated using the DFT/RB3LYP level of theory. (c) Changes in orbital energy level and electron density distribution of LUMO of $\text{Ni}(\text{II})(\text{itsq})_2$ (purple triangles) and HOMO of $\text{Ni}(\text{IV})(\text{dcpdt})_2$ (blue squares) by both proton and electron acceptances calculated at the DFT/RB3LYP level of theory. (d) Molecular structure with bond lengths (Å) of $\text{Ni}(\text{itsq})_2$ determined by X-ray diffraction (gray, C; white, H; blue, N; yellow, S; green, Ni).

atoms.

The crude product of $\text{Ni}(\text{itsq})_2$ was obtained under basic conditions according to the literature (see Supporting Information for details),^[11] and was characterized by ^1H NMR (Figure S2) and elemental analysis. Dark purple, plate-like single crystals were successfully grown by vapor diffusion of hexane into a dichloromethane solution at room temperature. Crystallographic analysis revealed that the complex molecules adopting a perfect square planar environment ($\tau_4 = 0$;^[12] Figure 1d) form a herringbone-like layered structure (Figure S3), as reported previously.^[13] In this molecule, the C–N bond (1.344(3) Å) is shorter than the single amino bond, whereas the C–S bond length (1.719(2) Å) is characteristic of a single bond. In addition, the C–C bond lengths in the benzene ring, i.e., two short bonds (1.365(3) and 1.375(3) Å) and four long bonds (1.403(3)–1.429(3) Å), affirmed the formation of an *o*-semiquinone-type structure. The bonding character was supported by infrared (IR) spectroscopy (Figure S4) and theoretical calculations, which also showed that protonation (i.e., $[\text{Ni}(\text{itsq})(\text{itsq}+\text{H})]^{1+}$) leads to elongation of the C–N bond (1.468 Å) and the aromatic nature of the benzene ring (1.391–1.408 Å). This structural change appears to be a manifestation of π -reconstruction of the ligand by protonation (Figure 1a). Magnetic susceptibility measurements revealed that the χT value (χ : magnetic susceptibility) at room temperature (0.034 emu K mol⁻¹; Figure S5) is significantly lower than the spin-only values of an $S = 1$ triplet spin (1.00 emu K mol⁻¹) or two $S = 1/2$ double spins (0.75 emu K mol⁻¹), possibly indicating the antiferromagnetic interactions between the radicals in the molecule. DFT calculations using the broken-symmetry

formalism^[14] showed that the broken-singlet state ($E_{\text{BS}} = -41867.10$ eV) is approximately 0.26 eV lower in energy than the triplet state ($E_{\text{T}} = -41866.84$ eV). The predicted energy difference affords a negative intramolecular exchange interactions with $J = -0.17$ eV using the Yamaguchi equation,^[15] as expected from the magnetic data.

The electronic absorption spectrum of $\text{Ni}(\text{itsq})_2$ in acetonitrile solution (0.10 mM) is shown in Figure 2a. The complex exhibited a distinct near-infrared (NIR) absorption band centered at 808 nm. A similar band was observed for neutral square-planar nickel complexes with semiquinone-type ligands.^[16] Time-dependent DFT (TD-DFT) calculations of the broken-singlet state were performed at the DFT/RB3LYP level of theory in acetonitrile solvent environment (Figure S6). As shown in Figure S6b, the calculated spectrum in the NIR region successfully reproduces the observed spectrum; the intense transition at 801.3 nm (oscillator strength $f = 0.4876$) involves the one-electron excitation from α -HOMO (ψ_{73}) to α -LUMO (ψ_{74}) (93.5%) as shown in the inset of Figures S6b and S7. Therefore, the 808-nm-band can be characterized as ligand-to-ligand charge transfer (LLCT) between itsq¹⁻ ligands to form atp-H^{2-} and itq^0 ligands (Figures S6a).^[10a,13]

To gain insight into the effect of protonation on electronic state, spectrophotometric titration experiments on 0.10 mM $\text{Ni}(\text{itsq})_2$ acetonitrile solution with an addition of acetonitrile solution of an anhydrous acid, bis(trifluoromethanesulfonyl)amine (HTf_2N) (0.068 M), were performed. The acid concentration in the reaction solution was estimated using the amount of added HTf_2N instead

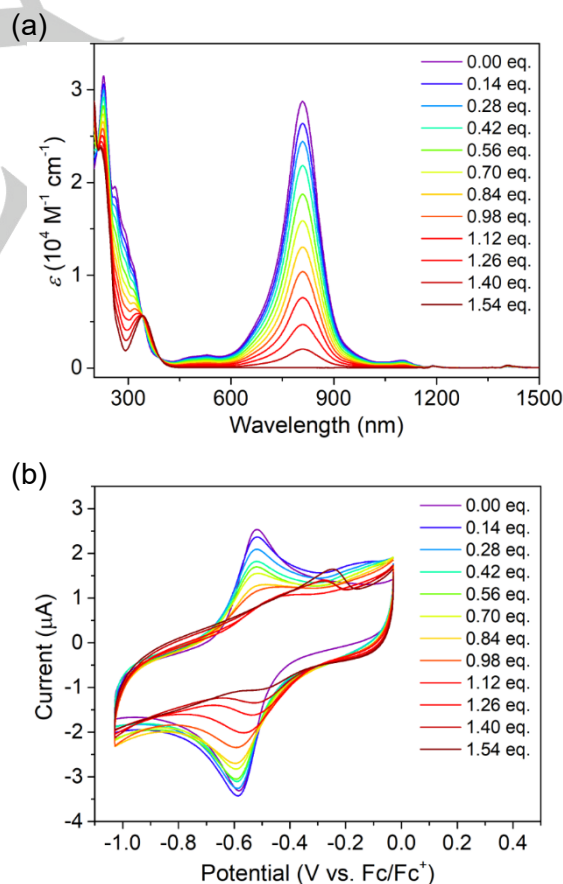


Figure 2. (a) UV-vis-NIR spectra during the titration of $\text{Ni}(\text{itsq})_2$ in acetonitrile solution (0.1 mM) using HTf_2N as the titrant. (b) Cyclic voltammograms during the titration of $\text{Ni}(\text{itsq})_2$ in acetonitrile solution (0.1 mM) containing $(\text{Bu}_4\text{N})\text{PF}_6$ using HTf_2N as the titrant.

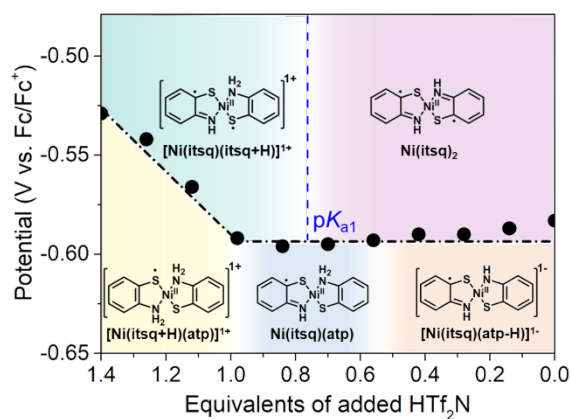


Figure 3. Pourbaix diagram of Ni(itsq)₂ complex system. Black circles indicate the potentials of the first reduction peak. A black dot-dashed line is a guide to the eye and a blue dotted line indicates pK_{a1} defined based on the spectrophotometric titration (see Figure S10). Diagram can be divided into five areas with different protonated and redox states (see text in details).

of the pH value, because of the poor solubility of Ni(itsq)₂ in water. The band was found to gradually weaken with the addition of HTf₂N and was eventually seen to disappear above 1.54 equiv. (Figure 2a). The disappearance of the 808-nm-band, which was supported by the TD-DFT calculation of the protonated structure, [Ni(itsq)(itsq+H)]¹⁺ (Figure S8), possibly arises from the low electron-donating ability of the protonated species, itsq+H⁰, in the complex molecule (see Figures 1a and S1).^[10a] The spectral change was accompanied by decolorization of the blue solution (Figure S9), and the intensity of the band was linearly correlated to the amount of added HTf₂N (Figure S10). Provided that the Ni(itsq)₂ species completely disappeared at 1.54 equiv., pK_{a1} can be defined for the equilibrium between Ni(itsq)₂ and [Ni(itsq)(itsq+H)]¹⁺ as the point with the half height of the absorbance (i.e., 0.76 equiv.).

The cyclic voltammogram (CV) was measured in a 0.1 mM Ni(itsq)₂ acetonitrile solution containing 0.10 M (Bu₄N)PF₆ as a supporting electrolyte. The complex showed two reversible couples at $E^{1/2} = -0.58$ V and $E^{1/2} = -1.43$ V vs. Fc/Fc⁺, which can readily be assigned to the first reduction from Ni(itsq)₂ to [Ni(itsq)(atp-H)]¹⁻ and the second reduction from [Ni(itsq)(atp-H)]¹⁻ to [Ni(atp-H)]₂²⁻, respectively (Figure S11).^[10b,10c,11] The reversible behavior was confirmed based on the square root dependence of the peak current (*i*_p) on the scan rate, i.e., *i*_p vs. (scan rate)^{1/2}, expected from the Randles-Sevcik equation (Figures S12 and S13).^[17] An initial titration of HTf₂N acetonitrile solution (0.068 M) had little effect on the redox potential below ca. 0.70 equiv., above which the redox couple showed a positive shift with a gradient of 220 mV equiv.⁻¹ (Figure 2b). According to the Nernst relationship for the PCET system under acidic conditions,^[18] such a redox shift is firm evidence of proton-coupled redox behavior in this system, providing a marked contrast with π-planar metal complexes with diiminosemiquinone ligands.^[9] The facile π-reconstruction of the ligand by protonation, which is associated with replacing imino groups to sulfur atoms, may be a reason for the increased proton–electron coupling. Notably, the amount of added HTf₂N that induces the acidity-dependent redox potential is in good agreement with that defined as the pK_{a1}. The potential–pH diagram (the so-called Pourbaix diagram) based on NIR absorption and CV data is shown in Figure 3. The initial species was readily assigned to pristine Ni(itsq)₂, which was

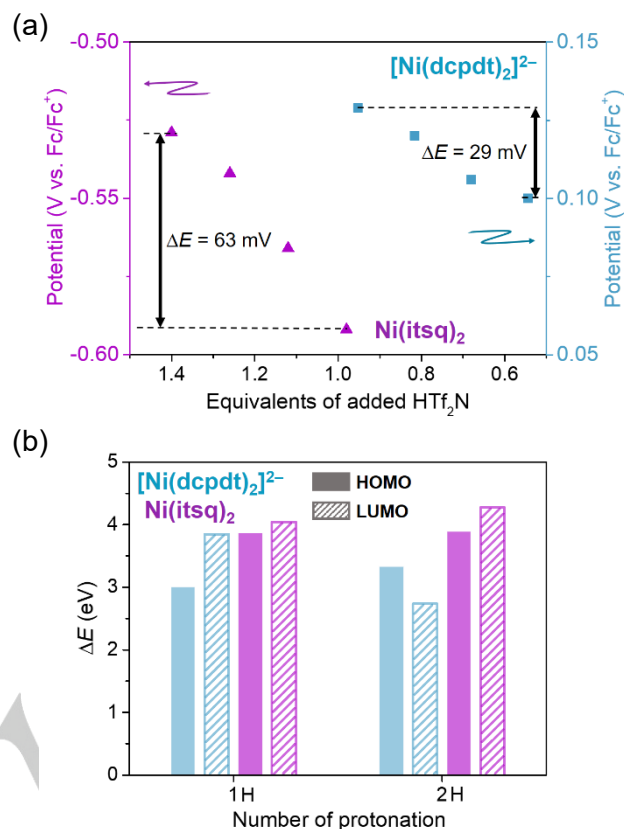


Figure 4. (a) Changes in first reduction potential of Ni(itsq)₂ (purple triangles) and first oxidation potential of [Ni(dcpdt)₂]²⁻ (blue squares) in the acidity-dependent redox potential region observed by CV measurements. (b) Stabilization in frontier orbital energy level (ΔE) of Ni(itsq)₂ (purple bars) and [Ni(dcpdt)₂]²⁻ (blue bars) by proton transfer calculated at the DFT/RB3LYP level of theory.

protonated at pK_{a1} (0.76 equiv.) to form the monoprotinated species, [Ni(itsq)(itsq+H)]¹⁺. The reduction of Ni(itsq)₂ with an acidity-independent redox potential provided a one-electron-reduced species, [Ni(itsq)(atp-H)]¹⁻. On the other hand, the reduced species of [Ni(itsq)(itsq+H)]¹⁺ through the acidity-dependent redox potential can be readily assigned to [Ni(itsq+H)(atp)]¹⁺; therefore, a neutral proton–electron transfer (PET) species, Ni(itsq)(atp), must be present between [Ni(itsq)(atp-H)]¹⁻ and [Ni(itsq+H)(atp)]¹⁺. It should be noted that the shift in the acidity-dependent redox potential (ca. 63 mV) is twice larger than that of [Ni(dcpdt)₂]²⁻ (ca. 29 mV; Figure 4a) with redox-inactive ligands, which was found to have the most stable PET state among the five types of pdt-based nickel complexes bearing various functional groups.^[4f] Given that the redox shift varies depending on the proton–electron coupling according to the Nernst equation,^[18] acid titration studies have demonstrated that the proton–electron coupling of Ni(itsq)₂ is more efficient than that of [Ni(dcpdt)₂]²⁻. Proton–electron coupling can also be theoretically evaluated by quantifying the energetic stabilization of frontier orbitals by protonation. Figure 4b shows the energetic stabilization of the frontier orbitals of Ni(itsq)₂ by protonation, together with those of [Ni(dcpdt)₂]²⁻ up to two protonated states, which were calculated at the DFT/RB3LYP level of theory. For [Ni(dcpdt)₂]²⁻, the stabilization energies of HOMO (blue solid bar) and LUMO (blue shaded bar) were estimated to be 3.2 and 3.3 eV, respectively, per protonation step. The stabilization of the

LUMO in Ni(itsq)₂ (4.2 eV per protonation step; purple shaded bar) is more pronounced than that of the HOMO in [Ni(dcpdt)₂]²⁻ (Figure S14), as expected from the electrochemical studies. In addition, the HOMO in Ni(itsq)₂ also shows significant stabilization by protonation (3.9 eV per protonation step; purple solid bar). This is possibly a consequence of the strong σ donation of sulfur atoms to central nickel ion, leading to extensive delocalization of the HOMO over the molecule. Such a delocalization of frontier orbitals, which are sensitive to the redox process on redox-active ligands, through metal–ligand coordination bonds, can pave the way for practical applications not only as iono-electronic materials,^[6] but also for catalytic reactions such as electrochemical and photochemical water oxidation.^[19]

In this study, a proton–electron coupled π -planar metal complex with redox-active *o*-aminobenzenethiolate ligands was investigated using experimental and theoretical approaches. Optical and electrochemical measurements demonstrated strong proton–electron coupling in the complex, which was manifested as significant acidity-sensitive reduction potential. Theoretical calculations predicted that proton–electron coupling in the complex, which was evaluated from the energetic shift of frontier orbitals by protonation, was more pronounced than that in a conventional nickel(II) complex with redox-inactive ligands. The judicious design of such redox-active ligands can tailor not only the redox properties but also the Lewis acidic/basic properties, and the eventual combination with metal ions can produce various metal complexes with the desired proton–electron coupling. Furthermore, the π -planar molecular structure provides a new pathway for designing coupled proton and electron conduction. Studies along this line are in progress.

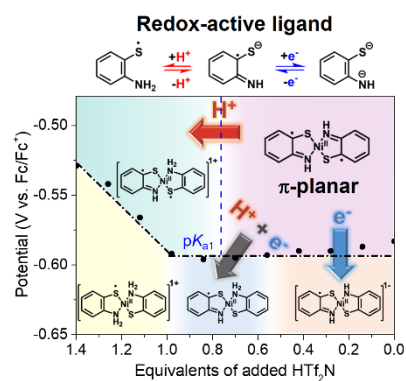
Acknowledgements

This work was supported by the ACCEL program (JPMJAC1501) of the Japan Science and Technology Agency (JST) and JSPS KAKENHI (Grant No. 18K05260, 20H02708, 20H05623, and 21K05004). The computations were performed using Research Center for Computational Science, Okazaki, Japan.

Keywords: nickel complex • redox-active ligand • proton–electron coupling • Pourbaix diagram • DFT calculations

- [1] a) H. Michel, J. Behr, A. Harrenga, A. Kannt, *Annu. Rev. Biophys. Biomol. Struct.* **1998**, *27*, 329–356; b) M. H. V. Huynh, T. J. Meyer, *Chem. Rev.* **2007**, *107*, 5004–5064; c) T. J. Meyer, M. H. V. Huynh, H. H. Thorp, *Angew. Chem. Int. Ed.* **2007**, *46*, 5284–5304; d) C. J. Gagliardi, B. C. Westlake, C. A. Kent, J. J. Paul, J. M. Papanikolas, T. J. Meyer, *Coord. Chem. Rev.* **2010**, *254*, 2459–2471; e) D. R. Weinberg, C. J. Gagliardi, J. F. Hull, C. F. Murphy, C. A. Kent, B. C. Westlake, A. Paul, D. H. Ess, D. G. McCafferty, T. Meyer, *Chem. Rev.* **2012**, *112*, 4016–4093.
- [2] a) T. Mitani, G. Saito, H. Urayama, *Phys. Rev. Lett.* **1988**, *60*, 2299–2302; b) K. Nakasuji, K. Sugiura, T. Kitagawa, J. Toyoda, H. Okamoto, K. Okaniwa, T. Mitani, H. Yamamoto, I. Murata, A. Kawamoto, J. Tanaka, *J. Am. Chem. Soc.* **1991**, *113*, 1862–1864; c) T. Murata, Y. Morita, Y. Yakiyama, K. Fukui, H. Yamochi, G. Saito, K. Nakasuji, *J. Am. Chem. Soc.* **2007**, *129*, 10837–10846; d) A. Ueda, S. Yamada, T. Isono, H. Kamo, A. Nakao, R. Kumai, H. Nakao, Y. Murakami, K. Yamamoto, Y. Nishio, H. Mori, *J. Am. Chem. Soc.* **2014**, *136*, 12184–12192; e) M. Shimozawa, K. Hashimoto, A. Ueda, Y. Suzuki, K. Sugii, S. Yamada, Y. Imai, R. Kobayashi, K. Itoh, S. Iguchi, M. Naka, S. Ishihara, H. Mori, T. Sasaki, M. Yamashita, *Nat. Commun.* **2017**, *8*, 1821.
- [3] R. Kato, *Chem. Rev.* **2004**, *104*, 5319–5346; b) T. Kusamoto, H. Nishihara, *Coord. Chem. Rev.* **2019**, *380*, 419–439.
- [4] a) T. Kubo, M. Ohashi, K. Miyazaki, A. Ichimura, K. Nakasuji, *Inorg. Chem.* **2004**, *43*, 7301–7307; b) M. Tadokoro, T. Inoue, S. Tamaki, K. Fujii, K. Isogai, H. Nakazawa, S. Takeda, K. Isobe, N. Koga, A. Ichimura, K. Nakasuji, *Angew. Chem. Int. Ed.* **2007**, *46*, 5938–5942; c) S. R. Kennedy, P. Goyal, M. N. Kozar, H. P. Yennawar, S. Hammes-Schiffer, B. J. Lear, *Inorg. Chem.* **2016**, *55*, 1433–1445; d) S. R. Kennedy, M. N. Kozar, H. P. Yennawar, B. J. Lear, *Inorg. Chem.* **2016**, *55*, 8459–8467; e) K. Koshiba, K. Yamauchi, K. Sakai, *Angew. Chem. Int. Ed.* **2017**, *56*, 4247–4251; f) Y. Kimura, M. Hayashi, Y. Yoshida, H. Kitagawa, *Inorg. Chem.* **2019**, *58*, 3875–3880; g) M. Hayashi, Y. Takahashi, Y. Yoshida, K. Sugimoto, H. Kitagawa, *J. Am. Chem. Soc.* **2019**, *141*, 11686–11693.
- [5] a) S. Sproules, K. Wieghardt, *Coord. Chem. Rev.* **2010**, *254*, 1358–1382; b) D. L. Broere, R. Plessius, J. I. van der Vlugt, *Chem. Soc. Rev.* **2015**, *44*, 6886–6915; c) N. P. van Leest, F. J. de Zwart, M. Zhou, B. de Bruin, *JACS Au* **2021**, *1*, 1101–1115.
- [6] a) P. Meredith, C. J. Bettinger, M. Irimia-Vladu, A. B. Mostert, P. E. Schwenn, *Rep. Prog. Phys.* **2013**, *76*, 034501; b) N. Amdursky, E. D. Glowacki, P. Meredith, *Adv. Mater.* **2019**, *31*, 1802221.
- [7] a) L. F. Warren, *Inorg. Chem.* **1977**, *16*, 2814–2819; b) D. Herebian, E. Bothe, F. Neese, T. Weyhermüller, K. Wieghardt, *J. Am. Chem. Soc.* **2003**, *125*, 9116–9128; c) D. Herebian, K. E. Wieghardt, F. Neese, *J. Am. Chem. Soc.* **2003**, *125*, 10997–11005.
- [8] a) T. Bugarcic, A. Habtemariam, R. J. Deeth, F. P. A. Fabbiani, S. Parsons, P. J. Sadler, *Inorg. Chem.* **2009**, *48*, 9444–9453; b) M. Kapovsky, C. Dares, E. S. Dodsworth, R. A. Begum, V. Raco, A. B. P. Lever, *Inorg. Chem.* **2012**, *52*, 169–181; c) T. Matsumoto, H.-C. Chang, M. Wakizaka, S. Ueno, A. Kobayashi, A. Nakayama, T. Taketsugu, M. Kato, *J. Am. Chem. Soc.* **2013**, *135*, 8646–8654; d) M. Yoshida, S. Ueno, Y. Okano, A. Usui, A. Kobayashi, M. Kato, *J. Photochem. Photobiol. A* **2015**, *313*, 99–106.
- [9] a) Y. Konno, N. Matsushita, *Bull. Chem. Soc. Jpn.* **2006**, *79*, 1046–1053; b) A. Masuya, N. Iki, C. Kabuto, Y. Ohba, S. Yamauchi, H. Hoshino, *Eur. J. Inorg. Chem.* **2010**, *2010*, 3458–3465.
- [10] a) A. Das, Z. Han, W. W. Brennessel, P. L. Holland, R. Eisenberg, *ACS Catal.* **2015**, *5*, 1397–1406; A. L. Balch, F. Röhrscheid, R. H. Holm, *J. Am. Chem. Soc.* **1965**, *87*, 2301–2302; c) E. I. Stiefel, J. H. Waters, E. Billig, H. B. Gray, *J. Am. Chem. Soc.* **1965**, *87*, 3016–3017.
- [11] R. H. Holm, A. L. Balch, A. Davison, A. H. Maki, T. E. Berry, *J. Am. Chem. Soc.* **1967**, *89*, 2866–2874.
- [12] L. Yang, D. R. Powell, R. P. Houser, *Dalton Trans.* **2007**, *9*, 955–964.
- [13] D. Herebian, E. Bothe, E. Bill, T. Weyhermüller, K. Wieghardt, *J. Am. Chem. Soc.* **2001**, *123*, 10012–10023.
- [14] a) L. Noodleman, *J. Chem. Phys.* **1981**, *74*, 5737–5743; b) L. Noodleman, E. R. Davidson, *Chem. Phys.* **1986**, *109*, 131–143; c) A. A. Ovchinnikov, J. K. Labanowski, *Phys. Rev. A* **1996**, *53*, 3946–3952.
- [15] K. Yamaguchi, F. Jensen, A. Dorigo, K. N. Houk, *Chem. Phys. Lett.* **1988**, *149*, 537–542.
- [16] a) D. V. Herebian, K. E. Wieghardt, F. Neese, *J. Am. Chem. Soc.* **2003**, *125*, 10997–11005; b) K. Ray, T. Weyhermüller, F. Neese, K. Wieghardt, *Inorg. Chem.* **2005**, *44*, 5345–5360; c) S. Blanchard, F. Neese, E. Bothe, E. Bill, T. Weyhermüller, K. Wieghardt, *Inorg. Chem.* **2005**, *44*, 3636–3656.
- [17] A. J. Bard, L. R. Faulkner, *Electrochemical Methods: Fundamentals and Applications*, 2nd ed. John Wiley & Sons, New York **2001**.
- [18] B. D. McCarthy, J. L. Dempsey, *Inorg. Chem.* **2017**, *56*, 1225–1231.
- [19] a) V. Lyaskovskyy, B. de Bruin, *ACS Catal.* **2012**, *2*, 270–279; b) O. R. Luca, R. H. Crabtree, *Chem. Soc. Rev.* **2013**, *42*, 1440–1459.

Entry for the Table of Contents



The strong proton–electron coupling behavior of a π -planar nickel(II) complex with redox-active N,S-ligands was demonstrated using optical and electrochemical methods as well as theoretical calculations. The potential–pH diagram shows a significant shift in the acidity-dependent redox potential, which is supported by the calculated energetic stabilization of frontier orbitals by protonation.